Available online at www.sciencedirect.com
SCIENCE DIRECT
Thermochimica Acta 440 (2006) 141–145
thermochimica acta
www.elsevier.com/locate/tca

Heat capacity measurements on uranium–cerium mixed oxides by differential scanning calorimetry

R. Venkata Krishnan, K. Nagarajan *

Pyrochemical Processing Studies Section, Fuel Chemistry Division, Chemistry Group, Indira Gandhi Centre for Atomic Research, Kalpakkam 603102, Tamilnadu, India

Received 12 July 2005; received in revised form 31 October 2005; accepted 3 November 2005
Available online 5 December 2005

Abstract

Uranium–cerium mixed oxides of three different compositions $(U_{0.2}Ce_{0.8})O_2$, $(U_{0.5}Ce_{0.5})O_2$ and $(U_{0.8}Ce_{0.2})O_2$, were prepared by combustion synthesis and characterized by XRD. The compositional characterization was done by ICP-AES. Heat capacity measurements employed a heat flux type differential scanning calorimeter from 280 to 820 K. The heat capacity values of $(U_{0.2}Ce_{0.8})O_2$, $(U_{0.5}Ce_{0.5})O_2$ and $(U_{0.8}Ce_{0.2})O_2$ at 298 K are 62.8, 64.2 and 70.1 $J\,K^{-1}\,mol^{-1}$, respectively. Enthalpy increment, entropy and Gibbs energy function were computed from the heat capacity data.

Keywords: Heat capacity; Differential scanning calorimetry; Thermodynamic properties; Uranium; Cerium; Mixed oxides

1. Introduction

Uranium–plutonium mixed oxides (MOX) are used as the fuel in fast breeder reactors. Cerium is one of the major fission products. Owing to its structural similarity CeO_2 readily forms solid solutions with UO_2 and PuO_2, the fuel constituents. Hence the thermodynamic properties of uranium–cerium mixed oxides are of interest. Cerium is also an inactive analogue for plutonium as the ionic radius of cerium and its chemical properties are very close to that of plutonium [1,2]. Experimental data on the heat capacity and enthalpy increments of uranium–plutonium mixed oxides are available only for a limited composition range, namely, 20% to 28% PuO_2 [3–11], though correlations by Fink [12], Cordfunke and Konings [13], MATPRO [14] and Carbajo et al. [15] exist for the estimation of enthalpy and heat capacity data. Since experimental data on the heat capacity of uranium–plutonium mixed oxides containing more than 28% PuO_2 are not available, data on uranium–cerium mixed oxides will be helpful in estimating the same for MOX fuels [2]. Most of the data available in the literature for the uranium–cerium mixed oxides are for the electrical conductivity [16], oxidation behaviour [2,17] oxygen potential [18,19], lattice parameter [19] and thermal expansion [20]. The only heat capacity data are of Arita et al. [21] for $(U_{0.91}Ce_{0.09})O_2$. In the present study, heat capacity measurements were carried out on the uranium–cerium mixed oxides $(U_xCe_{1-x})O_2$ ($x = 0.2, 0.5, 0.8$) in the temperature range 280–820 K by differential scanning calorimetry.

2. Experimental

2.1. Sample preparation

Uranium oxide of nuclear grade purity supplied by Nuclear Fuel Complex, Hyderabad, India, and CeO_2 of 99.9% purity supplied by M/s. Indian Rare Earths were used for preparing the samples. The solid solutions of urania and ceria were prepared by combustion synthesis, which uses the large exothermicity of the chemical reaction between the fuel and an oxidant to energize the synthesis [22–27]. In our preparation, citric acid was used as the fuel. The uranium oxide was heated at 1073 K for 4 h in a flowing stream of Ar + 8% H_2 mixture, which had been equilibrated with water at 298 K to convert it into $UO_{2.00}$ [28]. CeO_2 was heated in air at 673 K to remove any sorbed moisture. Stoichiometric quantities of UO_2 and CeO_2 thus treated were dissolved in nitric acid by heating at around 353 K. A drop of hydrofluoric acid was added to catalyze the solubility of CeO_2.

* Corresponding author. Tel.: +91 4114 280098; fax: +91 4114 280065.
E-mail address: knag@igcar.ernet.in (K. Nagarajan).

0040-6031/$ – see front matter © 2005 Elsevier B.V. All rights reserved.
doi:10.1016/j.tca.2005.11.005

Citric acid was added to the nitrate solution and mixed to get a clear solution. This mixture was then heated on a hot plate at 673 K. Combustion of the mixture took place with a flame. The resultant fine powder was ground, calcined at 1073 K in air for 4 h and compacted into pellets of 5 mm diameter with a hydraulic press. The pellets were heated at 1073 K for 4 h under a flowing stream of Ar + 8% H_2 gas equilibrated with water at 298 K to ensure that the O/M of the mixed oxide is 2.0 [28].

2.2. Sample characterization

Pellets of $(U_{0.2}Ce_{0.8})O_2$, $(U_{0.5}Ce_{0.5})O_2$ and $(U_{0.8}Ce_{0.2})O_2$ as well as those of CeO_2 and UO_2, from the same lot used for DSC measurements, were powdered and characterized by powder X-ray diffraction (XRD). The XRD patterns of the UO_2 and CeO_2 agreed well with those given in literature [1,29–33]. The XRD pattern of the solid solutions showed the absence of peaks due to pure UO_2 and pure CeO_2, confirming the formation of solid solution. Lattice parameters were derived from the XRD patterns of the uranium–cerium mixed oxides. The lattice parameters of $(U_{0.2}Ce_{0.8})O_2$, $(U_{0.5}Ce_{0.5})O_2$ and $(U_{0.8}Ce_{0.2})O_2$ were also computed from the lattice parameters of UO_2 and CeO_2 from literature[1,33], using Vegard's law. The two sets of lattice parameters are in good agreement (Table 1). The lattice parameters of $(U_{0.5}Ce_{0.5})O_2$ and $(U_{0.8}Ce_{0.2})O_2$ are also in good agreement with the values reported by Martin et al. [1] and Kim et al. [34].

Compositional characterization was done by inductively coupled plasma-atomic emission spectroscopy (ICP-AES). Accurately weighed amounts of UO_2, CeO_2, $(U_{0.2}Ce_{0.8})O_2$, $(U_{0.5}Ce_{0.5})O_2$ and $(U_{0.8}Ce_{0.2})O_2$ were dissolved in nitric acid. Ce (IV) was converted into Ce (III) by adding H_2O_2 during dissolution. Standard and sample solutions were 500–1000 ppm. Five sets of standard solutions for each element ranging from 5 to 25 ppm were prepared and used for calibration. The results of the analysis are: The concentrations of uranium in $(U_{0.2}Ce_{0.8})O_2$, $(U_{0.5}Ce_{0.5})O_2$ and $(U_{0.8}Ce_{0.2})O_2$ are 19.7, 49.1 and 80.9 mol% and those of cerium are 80.3, 50.9 and 19.1 mol%, respectively. The homogeneity of uranium and cerium within the pellet was ensured by SEM with EDAX. The results of compositional analysis by SEM-EDAX agree within ±1% with the expected values for all three solid solutions.

2.3. Calorimetric measurements

A heat flux type differential scanning calorimeter, model number DSC 821e/700 of M/s. Mettler Toledo GmbH, Switzerland, was used in this study. Temperature calibration was carried out by determining the melting temperatures of indium, tin, lead and zinc supplied by National Institute of Standards and Technology, USA (NIST), at heating rates of 2, 5, 10 and 20 K min^{-1}. The onset temperature of melting at different heating rates was plotted against the heating rate and extrapolated to zero heating rate. The extrapolated onset temperature at zero heating rate was used for temperature calibration. The calibration curve was obtained by fitting the difference between the known melting point of the calibration substances and the extrapolated onset temperatures to a second order polynomial. This provides instrument calibration under steady state condition.

The slope of melting point against heating rate curve gives the τ-lag, the difference between the time for the temperature sensor and sample to attain a given temperature under dynamic conditions. The calibration curve for the τ-lag was also obtained by fitting τ-lag at different temperatures to a second order polynomial. The typical value of τ-lag is 1–3 s.

Heat calibration was carried out by measuring the enthalpy of melting of indium, tin, lead and zinc at 10 K min^{-1}.

Heat rate calibration was performed prior to each heat capacity measurement with a disc of sapphire supplied by M/s. Mettler Toledo GmbH, Switzerland, using the heat capacity data of sapphire from NIST, USA.

Heat capacity measurements were carried out from 280 to 820 K. To eliminate any adsorbed moisture on the sample, the samples were heated to 573 K before starting the experiment. About 50–100 mg samples in the form of pellets were weighed accurately and hermetically sealed in 40 μL aluminum pans. The flow rate of the purge gas (ultra high pure argon) was 50 mL/min. A three-segment temperature program was used. The first segment was isothermal lasting for 5 min at the initial temperature; the second segment was from the initial temperature to the final temperature at a heating rate of 10 K min^{-1} and the final segment lasting for 5 min was again an isothermal one at the final temperature.

Each heat capacity measurement consisted of a set of three runs, namely, a blank run with empty pans on both sample and reference sides, a sapphire run with empty pan on the reference

Table 1
Room temperature lattice parameter of $(U_xCe_{1-x})O_2$

Compound	Lattice parameter (Å)		
	Computed using Vegard's law	Experimental	Literature data
UO_2	–	5.4719	5.4703 [29] 5.4705 [30] 5.4710 [31] 5.4700 [1]
CeO_2	–	5.4116	5.4110 [1,32,33]
$(U_{0.2}Ce_{0.8})O_2$	5.4229 [1,33]	5.4230	–
$(U_{0.5}Ce_{0.5})O_2$	5.4408 [1,33]	5.4337	5.4390 [1]
$(U_{0.8}Ce_{0.2})O_2$	5.4586 [1,33]	5.4577	5.4579 [34]

side and the pan with disc of sapphire on the sample side and finally the sample run with empty pan on the reference side and the sample in the form of pellet on the sample side.

3. Results

The heat capacity of UO_2 measured by DSC in the present work and given in Table 2 is the mean of five or six measurements. The relative standard deviations are 1–2%. The measured heat capacity of UO_2 was fitted to obtain the following polynomial in temperature by least squares

$$C_{p,m}\,(J\,K^{-1}\,mol^{-1}) = 75.466 + 0.0149\,T - 1443847\,T^{-2}\,(280–820\,K) \quad (1)$$

The standard error of the fit is $0.37\,J\,K^{-1}\,mol^{-1}$. The measured data along with the fit values are shown in Fig. 1. The heat capacity data of UO_2 reported in the literature [12,36–40], are also shown in Fig. 1. As can be seen, the present data are slightly higher (maximum 3%) than the literature data. The heat capacity data of $UO_{2.25}$ measured by Kurepin [41] are also shown in Fig. 1, which are much higher than the present as well as other literature data for stoichiometric UO_2.

The heat capacity of CeO_2 measured in the present work is given in Table 3. The relative standard deviations are 1–2%. The measured heat capacity of CeO_2 was fitted to obtain the following polynomial in temperature by least squares

$$C_{p,m}\,(J\,K^{-1}\,mol^{-1}) = 71.152 + 0.01335\,T - 1145425\,T^{-2}\,(280–820\,K) \quad (2)$$

The standard error of the fit is $0.59\,J\,K^{-1}\,mol^{-1}$. The measured data along with the fit values are shown in Fig. 2. The heat capacity data of Kuznetsov et al. [35] are given in Table 3 and are also shown in Fig. 2. As can be seen, the present data are slightly higher (2–4%) than those of Kuznetsov et al. [35].

The heat capacity of $(U_{0.2}Ce_{0.8})O_2$, $(U_{0.5}Ce_{0.5})O_2$ and $(U_{0.8}Ce_{0.2})O_2$ measured by DSC in the present work are given in Tables 4–6, respectively. The measured data are the mean of six to seven measurements and the relative standard deviation is ~3% for all three mixed oxides. The measured heat capacities of $(U_{0.2}Ce_{0.8})O_2$, $(U_{0.5}Ce_{0.5})O_2$ and $(U_{0.8}Ce_{0.2})O_2$ were fitted to a polynomial in temperature by least squares to give Eqs. (3)–(5), respectively. The measured data along with the fit values are given in Tables 4–6, respectively

$$C_{p,m}[(U_{0.2}Ce_{0.8})O_2]\,(J\,K^{-1}\,mol^{-1}) = 90.983 - 0.00169\,T - 2458865\,T^{-2}\,(280–820\,K) \quad (3)$$

$$C_{p,m}[(U_{0.5}Ce_{0.5})O_2]\,(J\,K^{-1}\,mol^{-1}) = 103.316 - 0.01077\,T - 3252155\,T^{-2}\,(280–820\,K) \quad (4)$$

Table 2
Heat capacity data for UO_2

T (K)	$C_{p,m}$ ($J\,K^{-1}\,mol^{-1}$)		
	Measured	Fit	Fink [12]
298	64.0	63.9	63.7
300	64.1	63.9	63.9
400	72.7	72.4	71.4
500	77.5	77.1	76.0
600	80.4	80.4	79.1
700	82.6	83.0	81.2
800	85.9	85.1	82.6

Table 3
Heat capacity data for CeO_2

T (K)	$C_{p,m}$ ($J\,K^{-1}\,mol^{-1}$)		
	Measured	Fit	Kuznetsov et al. [35]
298	62.6	62.0	61.5
300	62.7	62.4	61.7
400	68.8	69.3	67.1
500	73.0	73.3	70.6
600	76.5	76.0	73.3
700	78.6	78.2	75.7
800	79.3	80.1	77.8

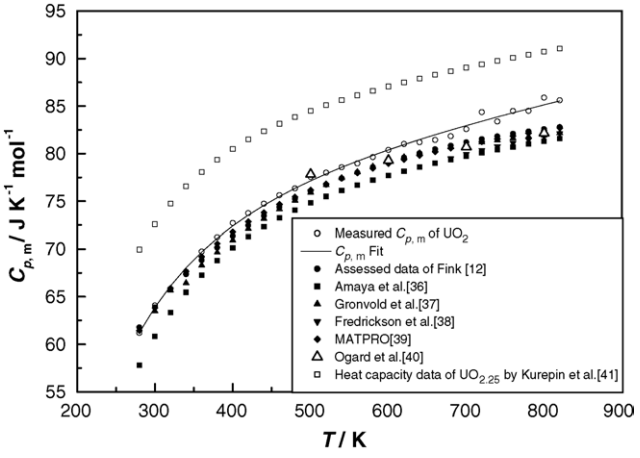

Fig. 1. Heat capacity data for UO_2.

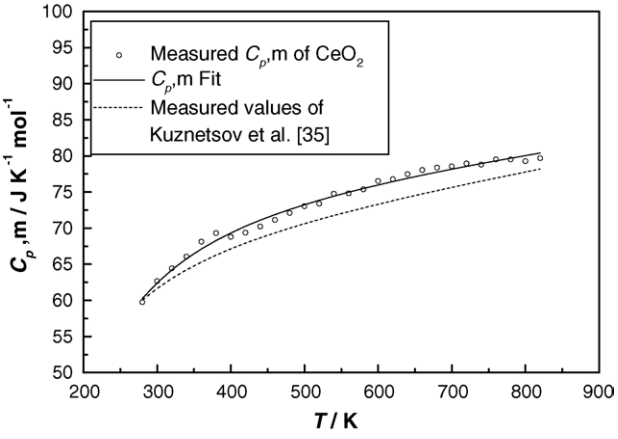

Fig. 2. Heat capacity data for CeO_2.

Table 4
Thermodynamic functions for $(U_{0.2}Ce_{0.8})O_2$

T (K)	$C_{p,m}$ (J K^{-1} mol^{-1})		$H^\circ_T - H^\circ_{298}$ (J mol^{-1})	S°_T (J K^{-1} mol^{-1})	$G^\circ_T - H^\circ_{298}/T$ (J K^{-1} mol^{-1})
	Measured	Fit			
298	62.8	62.8	0	69.4	−69.4
300	64.0	63.2	126	69.8	−69.4
400	73.3	74.9	7116	89.9	−72.1
500	81.2	80.3	14909	107.2	−77.4
600	84.6	83.1	23095	122.2	−83.7
700	84.5	84.8	31498	135.1	−90.1
800	85.2	85.8	40030	146.5	−96.5

Table 5
Thermodynamic functions for $(U_{0.5}Ce_{0.5})O_2$

T (K)	$C_{p,m}$ (J K^{-1} mol^{-1})		$H^\circ_T - H^\circ_{298}$ (J mol^{-1})	S°_T (J K^{-1} mol^{-1})	$G^\circ_T - H^\circ_{298}/T$ (J K^{-1} mol^{-1})
	Measured	Fit			
298	64.2	63.5	0	75.4	−75.4
300	64.8	63.9	118	75.8	−75.4
400	76.8	78.7	7362	96.6	−78.2
500	85.9	84.9	15583	114.9	−83.7
600	89.2	87.8	24238	130.7	−90.3
700	89.6	89.1	33096	144.3	−97.0
800	88.3	89.6	42039	156.2	−103.7

Table 6
Thermodynamic functions for $(U_{0.8}Ce_{0.2})O_2$

T (K)	$C_{p,m}$ (J K^{-1} mol^{-1})		$H^\circ_T - H^\circ_{298}$ (J mol^{-1})	S°_T (J K^{-1} mol^{-1})	$G^\circ_T - H^\circ_{298}/T$ (J K^{-1} mol^{-1})
	Measured	Fit			
298	70.1	69.9	0	78.3	−78.3
300	70.4	70.2	140	78.7	−78.3
400	79.7	80.7	7759	100.6	−81.2
500	86.0	85.8	16111	119.2	−87.0
600	88.9	88.7	24849	135.1	−93.7
700	90.3	90.7	33826	148.9	−100.6
800	92.0	92.1	42967	161.1	−107.4

$$C_{p,m}[(U_{0.8}Ce_{0.2})O_2]\,(J\,K^{-1}\,mol^{-1}) = 92.105 + 0.00402\,T - 2078914\,T^{-2}\,(280–820\,K) \quad (5)$$

4. Discussion

The data for all three mixed oxides are shown in Fig. 3. The heat capacity increases with increase in urania content because the heat capacity of UO_2 is higher than that of CeO_2. As can be seen from Fig. 3, the heat capacity data of all the mixtures are 10–15% higher than that estimated by Neumann–Kopp's law using the literature heat capacity data for UO_2 [12] and CeO_2 [35]. The only comparable heat capacity data hitherto reported in the literature are for $(U_{0.91}Ce_{0.09})O_2$ [21]. The present study covers a range of compositions from uranium rich to cerium rich.

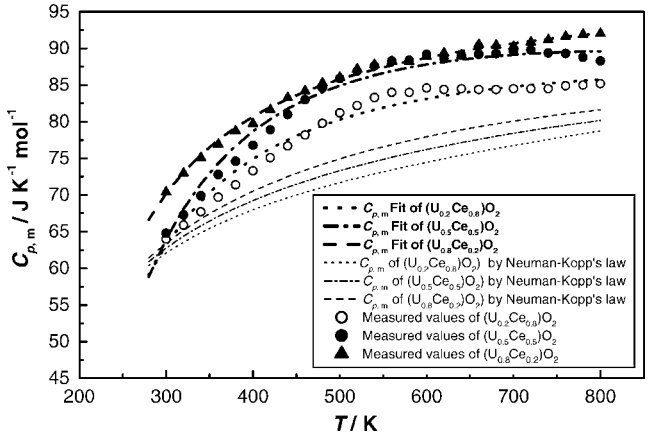

Fig. 3. Heat capacity data for $(U_{0.2}Ce_{0.8})O_2$, $(U_{0.5}Ce_{0.5})O_2$ and $(U_{0.8}Ce_{0.2})O_2$.

In addition to the trend of increasing heat capacity with increase in urania content, another feature is seen in Fig. 3. The heat capacity data for $(U_{0.5}Ce_{0.5})O_2$ show a plateau beginning around 600 K near the Debye temperature whereas that of $(U_{0.8}Ce_{0.2})O_2$ and $(U_{0.2}Ce_{0.8})O_2$ increase above this temperature, the increase being more pronounced in the former than the latter. The reasons for this are not understood. The increases cannot be attributed to the well-known polaron or point defect effects in the heat capacity of UO_2 [42,43], which are expected to only become significant above 1300 K.

From Eqs. (3)–(5), the enthalpy, entropy and Gibbs energy functions were computed and are given in Tables 4–6, respectively. The S°_{298} data of $(U_{0.2}Ce_{0.8})O_2$, $(U_{0.5}Ce_{0.5})O_2$ and $(U_{0.8}Ce_{0.2})O_2$, which are required for the computation of entropies, were estimated by adding the entropy of mixing to the value computed using the literature data for S°_{298} of pure UO_2 [12] and CeO_2 [35] by applying Neumann–Kopp's law.

Acknowledgements

The authors thank Dr. P.R. Vasudeva Rao, Director Chemistry Group and Dr. T.G. Srinivasan, Head, Fuel Chemistry Division, Indira Gandhi Centre for Atomic Research for their keen interest in this work. The authors wish to acknowledge the support of Ms. P.C. Clinsha, Project student from Mahatma Gandhi University, Kottayam. The authors also thank Mr. V. Srinivasan and Mr. P. Shankar of Indira Gandhi Centre for Atomic Research for ICP-AES and SEM analysis, respectively.

References

[1] P. Martin, M. Ripert, T. Petit, T. Reich, C. Hennig, F. D'Acapito, J.L. Hazemann, O. Proux, J. Nucl. Mater. 312 (2003) 103.
[2] H.P. Nawada, P. Sriramamurti, K.V.G. Kutty, S. Rajagopalan, R.B. Yadav, P.R. Vasudeva Rao, C.K. Mathews, J. Nucl. Mater. 139 (1986) 19.
[3] A.E. Ogard, J.A. Leary, Proceedings of the Symposium on Thermodynamics of the Nuclear Materials, IAEA, Vienna, 1967, p. 651.
[4] C. Affortit, J. Marcon, Rev. Int. Hautes Temp. Refract. 7 (1970) 236.
[5] D.G. Clifton, ILA-4749-MS, 1971. p. 28.
[6] L. Leibowitz, D.F. Fischer, M.G. Chasanov, J. Nucl. Mater. 42 (1972) 113.
[7] L. Leibowitz, D.F. Fischer, M.G. Chasanov, ANL-8082, 1974.
[8] R.L. Gibby, HEDL-TME-73-19, 1973.
[9] R.L. Gibby, L. Leibowtz, J.F. Kerrisk, D.G. Clifton, J. Nucl. Mater. 50 (1974) 155.
[10] M. Beauvy, J. Nucl. Mater. 188 (1992) 232.
[11] R. Kandan, R. Babu, K. Nagarajan, P.R. Vasudeva Rao, J. Nucl. Mater. 324 (2004) 215.
[12] J.K. Fink, J. Nucl. Mater. 279 (2000) 1.
[13] E.H.P. Cordfunke, R.J.M. Konings, Thermochemical Data for Reactor Materials and Fission Products, North-Holland, Amsterdam, 1990.
[14] MATPRO, A Library of Materials Properties for Light Water Reactor Accident Analysis, NUREG/CR-6150, vol. IV (INEL-96/0422), Rev. 1 October 1997.
[15] J.J. Carbajo, G.L. Yoder, S.G. Popov, V.K. Ivanov, J. Nucl. Mater. 299 (2001) 181.
[16] S.H. Kang, J.D. Yi, H. Yoo, S.H. Kim, Y.W. Lee, J. Phys. Chem. Solids 63 (2002) 773.
[17] K. Suresh Kumar, T. Mathews, H.P. Nawada, N.P. Bhat, J. Nucl. Mater. 324 (2004) 177.
[18] R. Ducroux, J. Baptiste, J. Nucl. Mater. 97 (1981) 333.
[19] D.I.R. Norris, P. Kay, J. Nucl. Mater. 116 (1983) 184.
[20] K. Yamada, S. Yamanka, M. Katsura, J. Alloys Compd. 275–277 (1998) 725.
[21] Y. Arita, T. Matsui, S. Hamada, Thermochim. Acta 253 (1995) 1.
[22] J.J. Moore, H.J. Feng, Prog. Mater. Sci. 39 (1995) 243.
[23] J.B. Holt, Z.A. Munir, J. Mater. Sci 21 (1986) 251.
[24] Z.A. Munir, Am. Ceram. Soc. Bull. 67 (1988) 342.
[25] C.R. Brown, B. Derby, Brit. Ceram. Trans. 96 (1997) 25.
[26] H.C. Yi, A. Pertric, J.J. Moore, J. Mater. Sci. 27 (1992) 6797.
[27] C.C. Hwang, T.Y. Wu, J. Wan, J.S. Tsai, Mater. Sci. Eng. B 111 (2004) 49.
[28] K. Nagarajan, R. Saha, R.B. Yadav, S. Rajagopalan, K.V.G. Kutty, M. Saibaba, P.R. Vasudeva Rao, C.K. Mathews, J. Nucl. Mater. 130 (1985) 242.
[29] L. Lynds, J. Inorg. Nucl. Chem. 24 (1972) 1007.
[30] J.A.C. Marples, in: H. Blank, R. Linder (Eds.), Proceedings of 5th International Conference on Plutonium and other Actinides, 1975, p. 353.
[31] A. Albinati, M.J. Cooper, K.D. Rouse, M.W. Thomas, B.T.M. Willis, Acta Cryst. A 36 (1980) 265.
[32] Y. Altas, H. Tel, J. Nucl. Mater. 298 (2001) 316.
[33] ASTM card no. 4-0556 and 4-0593, Powder diffraction file, sets 11-15, Inorganic vol. PDIS-15iRB, Published by Joint Committee on Powder Diffraction Standards, Swarthmore, PA, 1972.
[34] D.J. Kim, Y.W. Lee, Y.S. Kim, J. Nucl. Mater. 342 (2005) 192.
[35] F.A. Kuznetsov, T.N. Rezukina, A. Golushenko, Zhur. Fiz. Khin. 34 (1960) 101 (referred in O. Knacke, O. Knbaschewski, K. Hesselman. Thermochemical Properties of Inorganic Substances, second ed., Springer-Verlag, Berlin, 1991).
[36] M. Amaya, K. Une, K. Minato, J. Nucl. Mater 294 (2001) 1.
[37] F. Gronvold, N.J. Kveseth, A. Sveen, J. Tichy, J. Chem. Thermodyn. 2 (1970) 665.
[38] D.R. Fredrickson, M.G. Chasanov, J. Chem. Thermodyn. 2 (1970) 623.
[39] MATPRO, Version 11—A handbook of material properties for use in the analysis of light water reactor fuel rod behavior – NUREG/CR-0497.
[40] A.E. Ogard, J.A. Leary, Thermodynamics of Nuclear Materials, 1967, IAEA, Vienna, 1969, p. 651.
[41] V.A. Kurepin, J. Nucl. Mater. 303 (2002) 65.
[42] C. Ronchi, G.J. Hyland, J. Alloys. Compd. 213/214 (1994) 159.
[43] P. Ruello, L. Desgranges, G. Baldinozzi, G. Calvarin, T. Hansen, G. Petot-Ervas, C. Petot, J. Phys. Chem. Solids 66 (2005) 23.